# A Simplified Method to Measure the Diffusion Tensor from Seven MR Images

Peter J. Basser, Carlo Pierpaoli

**Analytical expressions of the diffusion tensor of water, $\underline{D}$, and of scalar invariants derived from it, are given in terms of the intensities of seven diffusion-weighted images (DWIs). These formulas simplify the post-processing steps required in diffusion tensor imaging, including estimating $\underline{D}$ in each voxel (from the set of b-matrices and their corresponding DWIs), and then computing its eigenvalues, eigenvectors, and scalar invariants. In a study conducted using artifact-free DWIs with high diffusion weighting ($b_{max} \sim 900$ s/mm$^2$), maps of Trace($\underline{D}$) and the Relative and Lattice Anisotropy indices calculated analytically and by multivariate linear regression showed excellent agreement in brain parenchyma of a healthy living cat. However, the quality of the analytically computed maps degraded markedly as diffusion weighting was reduced. Although diffusion tensor MRI with seven DWIs may be useful for clinical applications where rapid scanning and data processing are required, it does not provide estimates of the uncertainty of the measured imaging parameters, rendering it susceptible to noise and systematic artifacts. Therefore, care should be taken when using this technique in radiological applications.**

**Key words: MRI; diffusion; tensor; anisotropy.**

## INTRODUCTION

The Trace of the translational diffusion tensor, Trace($\underline{D}$), is proportional to the orientationally averaged water diffusivity (1) and is independent of the tissue's local fiber-tract direction (2). Its ability to demarcate ischemic regions in human stroke studies (3) as compared with apparent diffusion coefficient (ADC) imaging (4) should lead to its wide-spread use as an MR imaging parameter (2). However, Trace($\underline{D}$) is only one member of a family of useful "stains" that diffusion tensor MRI (2) provides to measure different intrinsic features or characteristics of water diffusion in tissues. These include the three principal diffusivities (eigenvalues), the three principal directions (eigenvectors), the three scalar invariants, and several indices of diffusion anisotropy, structural similarity, and tissue organization (2, 5, 6). Maps of the degree of diffusion anisotropy reveal organizational and architectural features of the normal human brain (7), as well as Wallerian degeneration of fibers in chronic stroke (8). The principal directions of $\underline{D}$ reveal additional organizational and architectural features in the brain (9–11), and in the heart (12, 13) that presently can not be elucidated using other imaging methods. In general, this new family of MRI parameters is expected to be useful in studying normal, pathological, developing, and aging tissues.

In the clinical environment, ensuring patient welfare and limiting the cost per scan behooves one to minimize the time required to obtain these imaging parameters. This entails both reducing the acquisition time of diffusion-weighted images (DWIs) and simplifying the subsequent data processing. To date, several simplified imaging schemes have been proposed to determine different quantities obtainable from the diffusion tensor using fewer than seven DWIs. For example, isotropically or Trace-weighted imaging schemes (14–16) produce images whose intensity is proportional to Trace($\underline{D}$) using as few as two DWIs. The tetrahedral gradient sampling scheme (17, 18) produces maps of Trace($\underline{D}$) and a diffusion anisotropy measure (18) using only five DWIs (but only by assuming that diffusion is cylindrically symmetric). Anisotropically weighted MRI schemes (19, 20) have been shown to require seven DWIs to produce an MRI whose intensity is an admissible measure of diffusion anisotropy in media where no *a priori* information on water diffusivity is available. Because seven DWIs is also the same number required to calculate the entire diffusion tensor analytically (21), it is prudent to investigate this special case and to examine its strengths and weaknesses.

## EXPERIMENTAL DESIGN

In diffusion tensor MRI, we estimate the effective diffusion tensor, $\underline{D}$, and the $T_2$-weighted echo amplitude, $A(\underline{b} = \underline{0})$, in each voxel from the MR echo attenuation and the applied gradient sequences using (21):

$$\ln\left(\frac{A(\underline{b})}{A(\underline{b} = \underline{0})}\right) = -\sum_{s=1}^{3}\sum_{t=1}^{3} b_{st} D_{st} = -\text{Trace}(\underline{b}\,\underline{D}) \quad [1]$$

Above, $\underline{b}$ is the $3 \times 3$ symmetric, positive semi-definite b-matrix; $\underline{D}$ is the corresponding $3 \times 3$ symmetric positive definite diffusion tensor; $\underline{b}\,\underline{D}$ is their matrix product; $A(\underline{b})$ is the echo amplitude measured using a pulse gradient sequence whose b-matrix is $\underline{b}$; and $A(\underline{b} = \underline{0})$ is the echo amplitude without diffusion attenuation. The b-matrix in Eq. [1] is calculated from the pulse gradient sequence as described elsewhere (22–24). In the special case in which seven DWIs are acquired with gradients applied in at least six noncollinear directions[1], Eq. [1] represents a system of seven linear equations and seven unknowns (six independent elements of $\underline{D}$ and $A(\underline{b} = \underline{0})$) whose values can be determined analytically (21).

**MRM 39:928–934 (1998)**

From the Tissue Biophysics and Biomimetics Section, NICHD (P.J.B.), and the Neuroimaging Branch, NINDS (C.P.), National Institutes of Health, Bethesda, Maryland.

Address correspondence to: Peter J. Basser, Ph.D., NIH/NICHD/STBB, Building 13, Room 3N-17, 13 South Drive, Bethesda, MD 20892-5766.

Received August 5, 1996; revised August 22, 1997; accepted September 2, 1997.

Work performed while P.J.B. was in the Biomedical Engineering and Instrumentation Program, NCRR.

0740-3194/98 $3.00



[1] with no three diffusion gradient vectors lying in the same plane

If we do not know the distribution of fiber orientations *a priori*, it is prudent to apply the diffusion gradient directions uniformly so as not to bias one's observations of molecular displacements along any one particular direction at the expense of others (7). Here, the first DWI is acquired with negligible diffusion weighting, whereas the remaining six DWIs are acquired with applied diffusion gradient vectors of equal magnitude and with a uniform orientational distribution. Specifically, we use a pattern of diffusion gradient directions such that the gradient vectors (and their reflections through the origin) pass through the vertices of a regular 14-sided polygon shown in Fig. 1 (7, 25). The gradient vector $\mathbf{G}^i$ contains the x, y, and z components applied during the $i^{th}$ DWI. $\mathbf{G}^i = G_0\,\mathbf{r}^i$ is the product of the peak diffusion gradient magnitude, $G_0$, and a unit (column) vector, $\mathbf{r}^i$, in the direction of the $i^{th}$ applied gradient vector:

$$\mathbf{G}^0 = \{0,\ 0,\ 0\}^T$$

$$\mathbf{G}^1 = G_0\left\{\frac{1}{\sqrt{2}},\ 0,\ \frac{1}{\sqrt{2}}\right\}^T;\quad \mathbf{G}^2 = G_0\left\{\frac{-1}{\sqrt{2}},\ 0,\ \frac{1}{\sqrt{2}}\right\}^T;$$

$$\mathbf{G}^3 = G_0\left\{0,\ \frac{1}{\sqrt{2}},\ \frac{1}{\sqrt{2}}\right\}^T \qquad [2]$$

$$\mathbf{G}^4 = G_0\left\{0,\ \frac{1}{\sqrt{2}},\ \frac{-1}{\sqrt{2}}\right\}^T;\quad \mathbf{G}^5 = G_0\left\{\frac{1}{\sqrt{2}},\ \frac{1}{\sqrt{2}},\ 0\right\}^T;$$

$$\mathbf{G}^6 = G_0\left\{\frac{-1}{\sqrt{2}},\ \frac{1}{\sqrt{2}},\ 0\right\}^T$$

To simplify the b-matrix, it is desirable to construct DWI sequences whose imaging gradients produce negligible diffusion attenuation (22). In this study, all such "cross terms" are almost entirely eliminated by refocusing imaging gradients just after they are applied, as has been described previously (26). Then, the b-matrix, $\underline{b}^i$, for the corresponding $i^{th}$ DWI, simplifies to the form reported previously (21):

$$\underline{b}^i = \alpha^2\,\mathbf{G}^i\,\mathbf{G}^{iT} = \alpha^2 G_0{}^2\,\mathbf{r}^i\,\mathbf{r}^{iT} \qquad [3]$$

where $\alpha$ is a constant that depends only on the proton gyromagnetic ratio, the gradient pulse sequence shape and duration, and other timing parameters (21). With Eq. [3], we can simplify the relationship between the $i^{th}$ log-ratio image, $IM_i$, and the corresponding diffusion gradient sequence from

$$IM_i = \ln\left(\frac{A(\underline{b}^i)}{A(\underline{b}^0 = \underline{0})}\right) = -\sum_{s=1}^{3}\sum_{t=1}^{3} b^i_{st}\,D_{st} \qquad [4]$$

to

$$IM_i = \ln\left(\frac{A(\mathbf{G}^i)}{A(\mathbf{G}^0 = \mathbf{0})}\right) = -\alpha^2\,G_0{}^2\,\mathbf{r}^{iT}\,\underline{D}\mathbf{r}^i$$

$$= -\alpha^2 G_0{}^2 \sum_{s=1}^{3}\sum_{t=1}^{3} r^i_s\,r^i_t\,D_{st} \qquad [5]$$

Then, $IM_i$ has a simple interpretation: it is proportional to the apparent diffusion coefficient (ADC) measured along the direction $\mathbf{r}^i$.

By substituting the seven gradient vectors given in Eq. [2] into Eq. [5], we obtain six independent equations for the $IM_i$ that are linear functions of the six independent elements of the diffusion tensor: $D_{xx}$, $D_{xy}$, $D_{xz}$, $D_{yy}$, $D_{yz}$, and $D_{zz}$. This system of linear equations is solved simultaneously, yielding analytical expressions for each of the six diffusion tensor elements:

$$D_{xz} = \frac{-IM_1 + IM_2}{4b},\quad D_{yz} = \frac{-IM_3 + IM_4}{4b},$$

$$D_{xy} = \frac{-IM_5 + IM_6}{4b}$$

$$D_{zz} = \frac{-IM_1 - IM_2 - IM_3 - IM_4 + IM_5 + IM_6}{4b} \qquad [6]$$

$$D_{xx} = \frac{-IM_1 - IM_2 + IM_3 + IM_4 - IM_5 - IM_6}{4b}$$

$$D_{yy} = \frac{IM_1 + IM_2 - IM_3 - IM_4 - IM_5 - IM_6}{4b}$$

Above, we have used the definition $b = (\frac{1}{2})\alpha^2 G_0{}^2$. Effectively, from the measurement of ADCs applied in six directions, we are able to determine each of the six diffusion tensor elements. However, the six independent elements of the diffusion tensor are now expressed explicitly in terms of the six IMs.

Using Eq. [6], we can obtain an analytical expression for any function of $\underline{D}$ in terms of the log-ratio images. For example, analytical expressions can be obtained for the

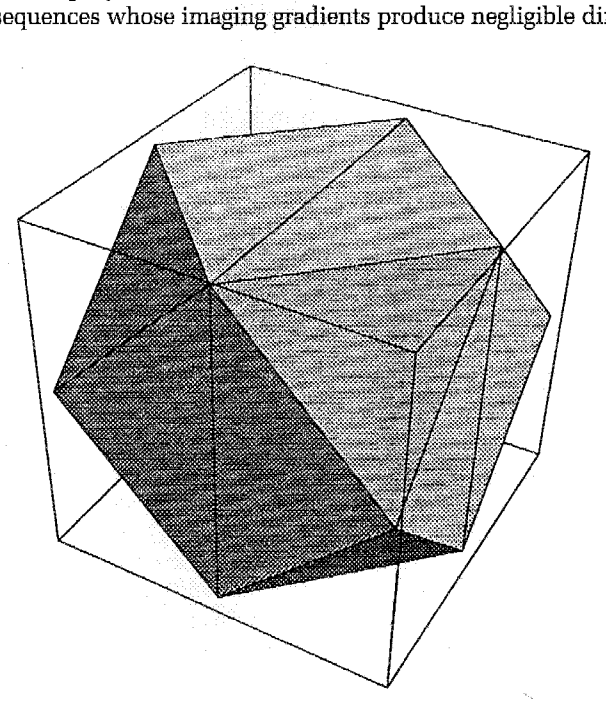

FIG. 1. A 14-sided regular polyhedron used to represent the diffusion gradient directions applied in this study. The gradient vectors and their reflections through the origin pass through the vertices of this polyhedron. The six-gradient independent gradient vectors consist of three pairs of orthogonal vectors.

three principal diffusivities of $\underline{D}$, $\lambda_1$, $\lambda_2$, and $\lambda_3$, by solving the characteristic equation of $\underline{D}$. Their formulas can be obtained in ref. 27. The eigenvectors of $\underline{D}$ generally are solved analytically or numerically once the eigenvalues are determined (e.g., see refs. 27 and 28). The three scalar invariants of $\underline{D}$, $J_1$, $J_2$, and $J_3$, can be calculated directly from $\underline{D}$ using the formulas:

$$J_1 = \text{Trace}(\underline{D})$$

$$J_2 = \frac{1}{2}(\text{Trace}(\underline{D})^2 - \text{Trace}(\underline{D}^2)) \qquad [7]$$

$$J_3 = \text{Determinant}(\underline{D})$$

## EXPERIMENTAL METHODS

Diffusion-weighted MRIs (DWIs) of live healthy anesthetized cat brains were obtained using a 2-T CSI animal imaging system (35 cm bore) and a birdcage quadrature coil (13 cm id). One DWI with $\mathbf{G}^0 = \{0, 0, 0.3\}$ G/cm was acquired to approximate $A(\mathbf{G}^0 = \mathbf{0})$, the DWI with no diffusion weighting. Subsequently, diffusion gradients were applied in six oblique directions according to the scheme given in Eq. [2] above. Four different levels of diffusion weighting were used. These four sets of six DWIs were acquired with $G_0 = 1.5$ G/cm, 2.13 G/cm, 2.61 G/cm, and 3.0 G/cm. A total of 25 (128 × 128) axial, four-slice, interleaved DW navigator corrected echo-planar images (EPI) (29, 30), were acquired in 40 min. Using only seven DWIs reduces the acquisition time to about 11 min. Additional imaging parameters were: TE = 75.62 ms, $\Delta$ = 38.85 ms, $\delta$ = 14 ms, TR = 3 s, na = 2, FOV = 80 mm, st = 2.5 mm (slice thickness), number of interleaves = 16. The diffusion weighting of the four sets of DWIs was given by $\text{Trace}(\underline{b})$ = 228.82, 461.402, 692.79, and 915.3 s/mm$^2$.

We then used Eq. [6] to calculate $\underline{D}$ in each voxel for each of the four sets of six DWIs and the single image, $A(\mathbf{G}^0 = \mathbf{0})$. For comparison, we also used the entire set of 25 DWIs and their calculated b-matrices, to determine $\underline{D}$ and $A(\underline{b} = \underline{0})$ in each voxel from Eq. [4] using multivariate linear regression (2). The performance of the analytically derived and statistically estimated diffusion tensor maps were then compared, as described below.

## RESULTS

The first scalar invariant, $\text{Trace}(\underline{D})$, can be expressed as the sum of the logarithm of the attenuation of six DWIs:

$$\begin{aligned}\text{Trace}(\underline{D}) &= D_{xx} + D_{yy} + D_{zz} \\ &= 3\langle D\rangle \\ &= -\frac{1}{4b}(IM_1 + IM_2 + IM_3 + IM_4 + IM_5 + IM_6)\end{aligned} \qquad [8]$$

Above, $D_{xx}$, $D_{yy}$, and $D_{zz}$ are the three diagonal elements of the diffusion tensor, and $\langle D\rangle$ is their average—the mean diffusivity. Figures 2a to 2d show $\text{Trace}(\underline{D})$ calculated from Eq. [8] using $A(\mathbf{G}^0 = \mathbf{0})$ and four sets of six DWIs with increasing amounts of diffusion weighting in each set. Figure 2e shows $\text{Trace}(\underline{D})$, where $\underline{D}$ is estimated from the pooled set of 25 DWIs by using multivariate linear regression of Eq. [1] (21, 23). Figure 2f shows the $T_2$-weighted image, $A(\underline{b} = \underline{0})$, also estimated from the entire set of 25 DWIs using Eq. [1].

One measure of diffusion anisotropy derivable from $\underline{D}$ is the relative anisotropy (RA) index, defined previously as (5):

$$RA = \frac{\sqrt{3}}{1}\frac{\sqrt{\text{Trace}((\underline{D} - \langle D\rangle \underline{I})^2)}}{\text{Trace}(\underline{D})} \qquad [9]$$

where $\underline{I}$ is the identity matrix. RA is the ratio of the magnitudes of the anisotropic and isotropic parts of the diffusion tensor, respectively. Figures 3a to 3d show RA calculated from $A(\mathbf{G} = \mathbf{0})$ and from each of the four sets of six DWIs with increasing diffusion sensitization, whereas Fig. 3e shows RA calculated from $\underline{D}$ that is estimated from the pooled data set using all 25 DWIs. Figure 3f again shows $A(\underline{b} = \underline{0})$ estimated from the pooled data set, using all 25 DWIs for comparison. It should be noted that the expression for RA is independent of the value of b.

A more noise-immune and less-biased measure of diffusion anisotropy than RA is the lattice anisotropy index (6), whose application to human brain imaging has recently been demonstrated (7). Figures 4a to 4d show the lattice index calculated from $A(\mathbf{G}^0 = \mathbf{0})$ and from each of the four sets of six DWIs with increasing diffusion sensitization, whereas Fig. 4e shows the lattice anisotropy index calculated from $\underline{D}$ that is estimated from the pooled data set using all 25 DWIs. Figure 4f again shows $A(\underline{b} = \underline{0})$ estimated from the pooled data set.

## DISCUSSION

Although the formulas given in Eq. [6] apply to the log-ratio images (IMs) obtained using the particular gradient pattern given in Eq. [2], in principle, any set of seven DWIs will yield an exact expression for $\underline{D}$. The only requirement is that the six gradient vectors not all lie in the same plane and that no two gradient vectors are collinear[2]. Although other gradient patterns may provide higher SNR per unit time or per image, the gradient scheme used here achieves a high SNR per image while sampling gradient directions uniformly (7).

Recall that $\text{Trace}(\underline{D}) = J_1$ is proportional to the diffusivity averaged uniformly over all directions (1). Examining Eq. [8] reveals that when the gradient directions are sampled uniformly (as in Eq. [2]), we produce an isotropically or "Trace"-weighted MRI simply by summing the six IMs. This is because each IM is proportional to the ADC in the direction along which the diffusion gradients are applied. Because the six directions given in Eq. [2] are spherically or isotropically distributed, averaging the six IMs represents a discrete orientational average of the six ADCs. A similar result was shown recently when diffusion-gradient directions were arranged with tetrahedral

[2] These conditions will guarantee that Eq. [5] results in a full-rank matrix that is invertible.

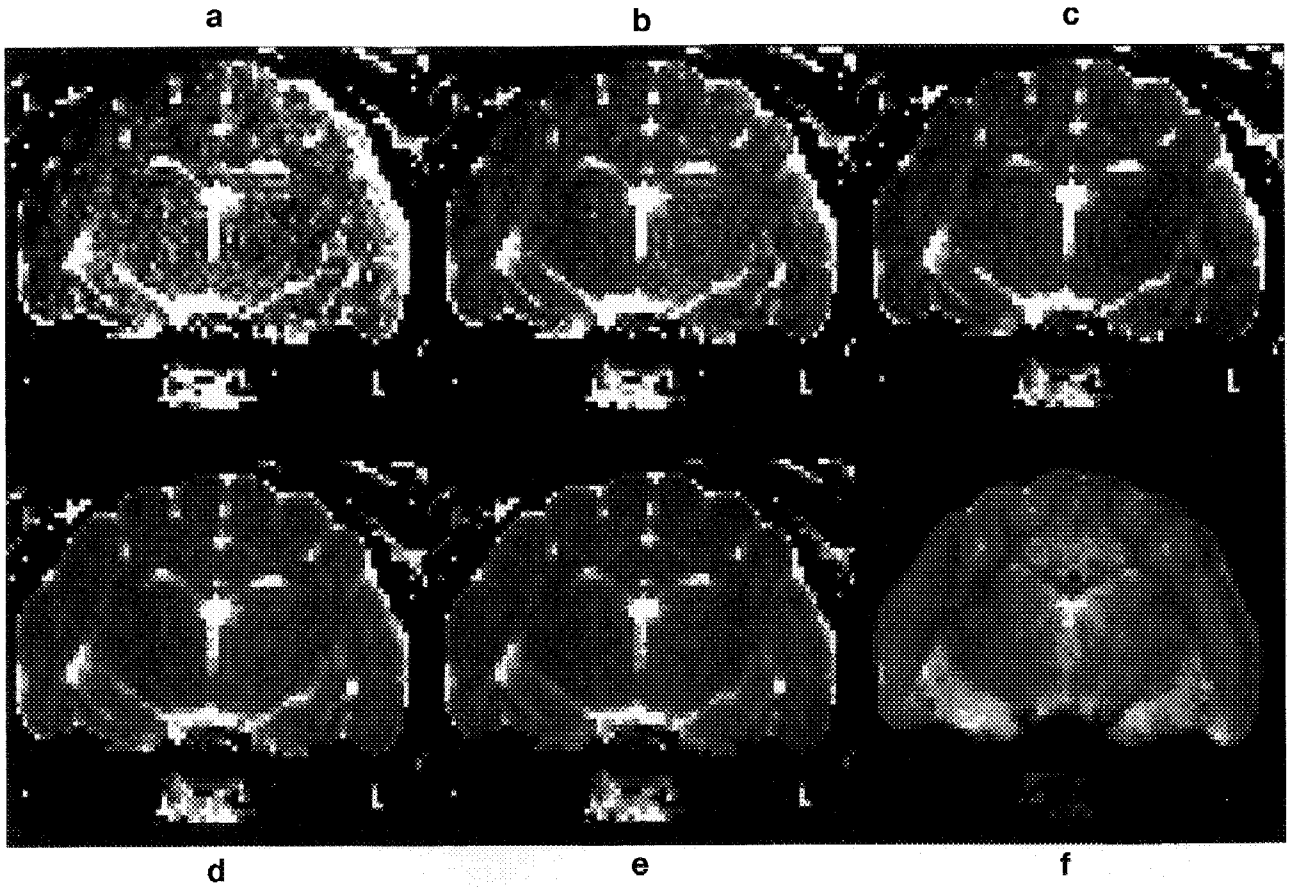


FIG. 2. Trace(D) in healthy cat brain. The first four images are calculated using only seven DWIs, using Eq. [8], with the gradient pattern given in Eq. [6]. Images (a) to (d) are acquired with different levels of diffusion weighting, i.e., Trace(b) = (a) 228.82 s/mm$^2$; (b) 461.402 s/mm$^2$; (c) 692.79 s/mm$^2$; and (d) 915.3 s/mm$^2$. Juxtaposed are the images of (e) Trace(D) and (f) A(b = 0), which were both estimated statistically from the entire data set of 25 DWIs, using Eq. [1].

symmetry (18, 31) and in general is predicted to hold for all schemes in which gradient directions are isotropically oriented (uniformly distributed), and in which diffusion gradient amplitudes are also uniform. Interestingly, the formulas for all three scalar invariants, $J_1$, $J_2$, and $J_3$ are independent of the order in which the six (nonzero) gradients are applied.

A strength of performing diffusion tensor MRI using seven DWIs is that by providing exact solutions for all the diffusion tensor elements (as well as for any quantities derived from them), one reduces the complexity of post-processing the DWIs. Specifically, these formulas obviate the steps of calculating the b-matrix from each DWI sequence and estimating the diffusion tensor from a set of these DWIs. These steps are all subsumed in the functional relationships between the logarithms of seven DWIs and D (see Eq. [6]). Another advantage is that total scan time required to perform diffusion tensor MRI is reduced by minimizing the number of acquired DWIs.

Surprisingly, one can obtain comparable image quality when using only seven DWIs, as one obtains using a much larger number of DWIs if care is taken in experimental design and in its execution (as described below). For example, good agreement is found between all Figs. marked "d" and "e", even though the former were obtained using only seven DWIs and the latter were obtained using 25 DWIs.

One of the most promising uses of diffusion tensor MRI with seven DWIs is in analyzing and planning DT-MRI experiments with more than seven DWIs (2). The first seven DWIs can be used to furnish maps of D, A(b = 0), Trace(D) (or ⟨D⟩), diffusion anisotropy indices, principal diffusivities, and principal axes. These initial estimates can then be updated and refined after the acquisition of each subsequent DWI. Second, the exact solutions for D and of A(b = 0) can be used in "boot-strap" procedures (27) to estimate the distributions of D, A(b = 0), and quantities derived from them, from a set of more than seven DWIs. Finally, in an experiment in which D is expected to change rapidly with time, such as during acute ischemia, it may be advantageous to continuously acquire repetitive sets of seven DWIs. For the highest temporal resolution, D and other quantities derived from it can be calculated at each time point by using only seven contiguous DWIs. A similar approach was used to follow the kinetic behavior of Trace(D) and the principal diffusivities during hyperacute ischemia (32).

However, several assumptions must be satisfied to use this simplified imaging method with confidence. First, to obtain such simple algebraic expressions for D (and for its

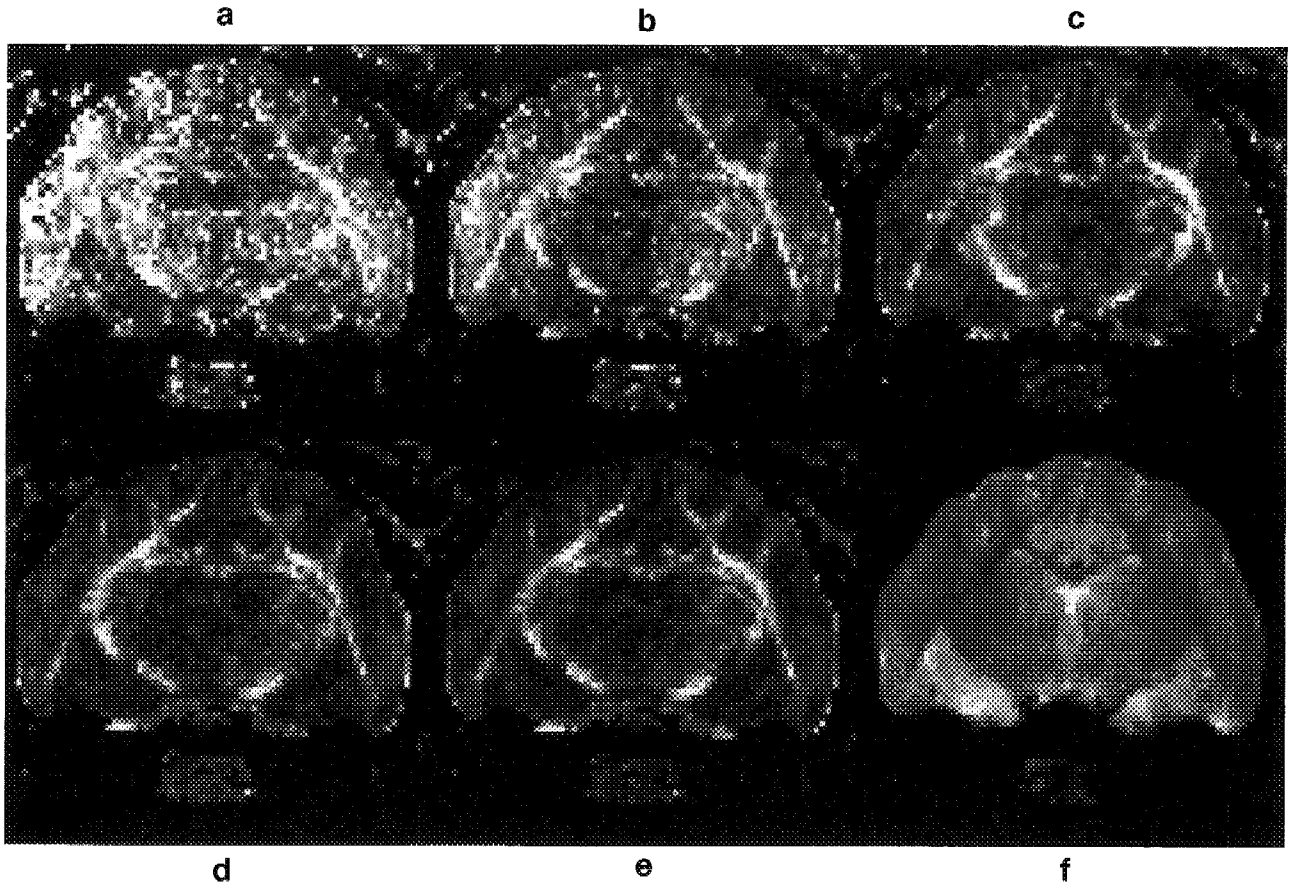


FIG. 3. The relative anisotropy (RA) index map in healthy cat brain. The first four RA images are calculated from seven DWIs, using Eq. [9] with the gradient pattern given in Eq. [2]. Images (a) to (d) are acquired with different levels of diffusion weighting, i.e., Trace($\underline{b}$) = (a) 228.82 s/mm$^2$; (b) 461.402 s/mm$^2$; (c) 692.79 s/mm$^2$; and (d) 915.3 s/mm$^2$. Juxtaposed are the images of (e) RA and (f) A($\underline{b}$ = $\underline{0}$), which were both estimated statistically from the entire data set of 25 DWIs, using Eq. [1].

invariants), we neglect the contributions of the imaging gradients on the signal attenuation. This is justified in our case because the DWI sequences were designed so that all cross-terms (22, 23, 26, 33) would be negligibly small. We calculated the b-matrix for each echo-planar DWI numerically and verified that imaging gradients contributed less than 1% to the total signal attenuation. Even if imaging gradients were significant, they still could be accounted for, and exact expressions for $\underline{D}$ and its invariants could be found, albeit, these expressions would be more complicated than the ones presented here. Second, we assume that when we acquire the A($\mathbf{G}^0 = \mathbf{0}$) image, there is no diffusion attenuation. In practice, the A($\mathbf{G}^0 = \mathbf{0}$) sequence generally contains small crusher gradients that introduce some diffusion attenuation, but in our case, their effect was negligibly small, because their maximum contribution to Trace($\underline{b}$) was 4.57 s/mm$^2$. Third, this method assumes that the DWIs are all free of noise. In Figs. 2a to 2d and 3a to 3d, we see the progressive, deleterious effect of noise on Trace($\underline{D}$) and RA as diffusion weighting is reduced. It is a well-known result that for a process with a high SNR, exhibiting a simple exponential decay, an optimal sampling strategy is to make two observations, one at the initial value and a second at a time equal to the exponential time constant. An analogous situation exists in estimating the apparent diffusion constant and the diffusion tensor (although the situation is further complicated in the MR experiment by $T_1$ and $T_2$ relaxation (34)). Crudely, an optimal estimate of the mean diffusivity $\langle D \rangle$ is obtained when

$$1 \sim \text{Trace}(\underline{b})\langle D \rangle \qquad [10]$$

Because, for brain parenchyma, $\langle D \rangle \sim 700 - 800 \times 10^{-6}$ mm$^2$/s (6, 7), the optimal Trace($\underline{b}$) $\sim$ 1400 s/mm$^2$. It is not surprising, therefore, that our results are best with Trace($\underline{b}$) = 2 b = 915 s/mm$^2$ and degrade progressively as diffusion weighting decreases. Fourth, this method assumes that the DWIs are free of systematic artifacts, in particular: (1) ghosting caused by motion; (2) signal attenuation due to additional background gradients, or magnetic susceptibility variations; (3) image distortion due to induced eddy-currents; (4) improperly calibrated gradients; and (5) magnetic field inhomogeneity. In this study, care was taken to mitigate all of these systematic artifacts although they were not all entirely eliminated. Of those mentioned above, motion artifacts are usually the most serious in a clinical environment. They were reduced here by sedating the animal and by using navigator-echo–corrected DWI sequences. As diffusion weighting decreases from Trace($\underline{b}$) = 915.3 to 228.82 s/mm$^2$, systematic artifacts are progressively more apparent near the skull. In Fig. 2a, a dark band appears on the

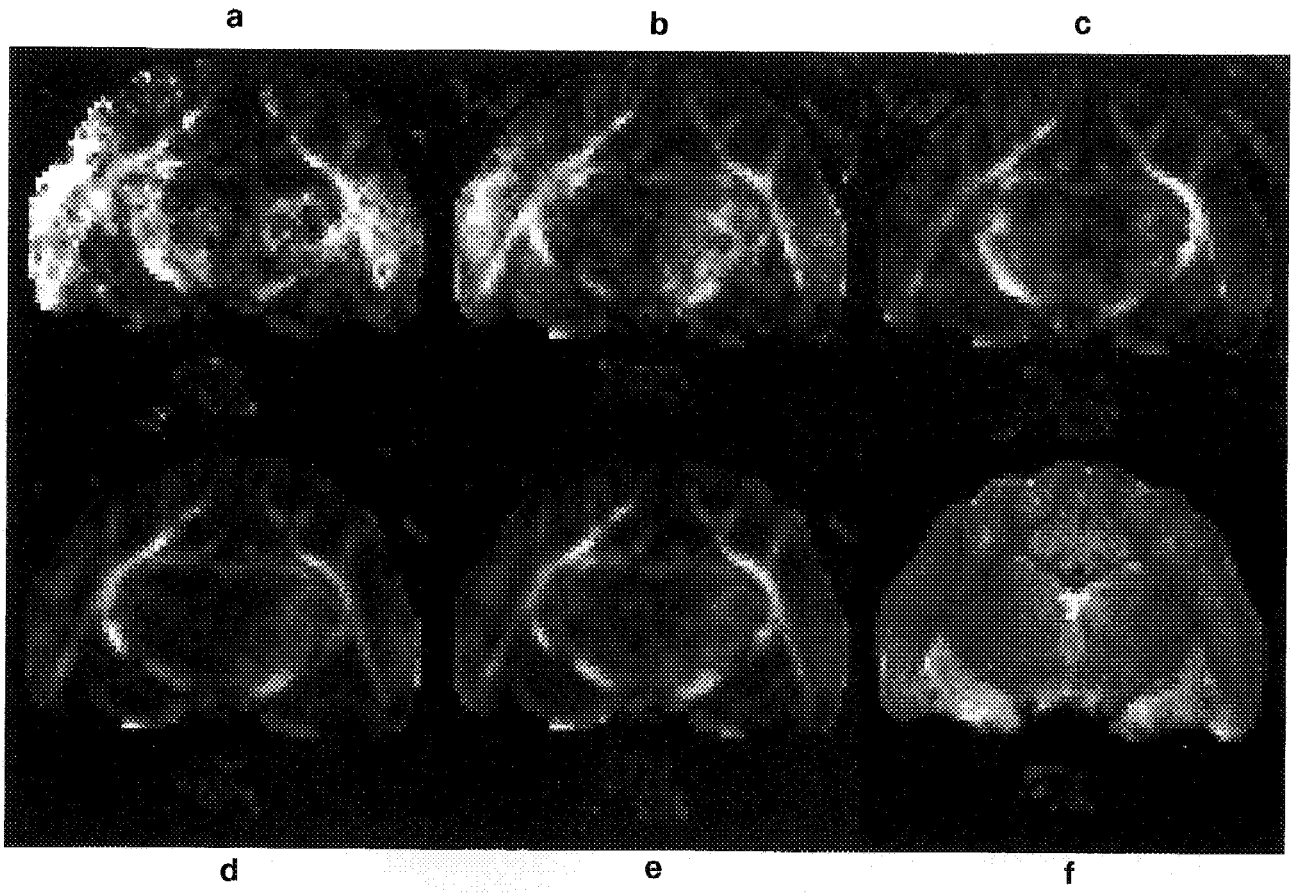


FIG. 4. The lattice anisotropy index map in healthy cat brain. The first four images are calculated from seven DWIs, with the gradient pattern given in Eq. [2]. Images (a) to (d) are acquired with different levels of diffusion weighting, i.e., Trace($\underline{b}$) = (a) 228.82 s/mm$^2$; (b) 461.402 s/mm$^2$; (c) 692.79 s/mm$^2$; and (d) 915.3 s/mm$^2$. Juxtaposed are the images of (e) the lattice anisotropy index and (f) A($\underline{b} = \underline{0}$), which were both estimated statistically from the entire data set of 25 DWIs, using Eq. [1]. Comparing Figs. 3 and 4, we see that at each level of diffusion weighting, the lattice anisotropy index significantly reduces the noise level and more clearly depicts the fiber tracts. However, in the images in which systematic artifacts are evident, i.e., in (a) and (b), the lattice anisotropy index does not suppress them.

left cortex, and a bright band appears on the right cortex, which are successively less conspicuous as diffusion attenuation increases in Figs. 2b to 2d. In the clinic, systematic artifacts are expected to be more pronounced, and it is likely that one or more of the seven DWIs may be corrupted by motion. One should note that assumptions 2, 3, and 4 above apply to all isotropically weighted imaging sequences proposed to date (14–16), to the tetrahedral method (18, 31), as well as to the new anisotropically weighted imaging schemes proposed recently (20), so a comparably level of care should be taken in using these methods as well.

There are also drawbacks to using these simplified imaging schemes. For instance, when we acquire more than seven DWIs to determine the diffusion tensor, we also obtain estimates of the means and variances of $\underline{D}$ and A($\underline{b} = \underline{0}$), as well as of the quantities derived from them (21). However, diffusion tensor MRI using only seven DWIs is a deterministic, not a statistical procedure, so no such estimates can be obtained. This limitation precludes us from assigning confidence levels for the imaging parameters we calculate, and from determining a meaningful measure of goodness of fit of the model to the data, because for seven equations and seven unknowns, the fit is always perfect. Generally, the absence of additional degrees of freedom makes our results more susceptible to systematic artifacts and noise, because with additional images, one can ameliorate these effects, for example, by weighting images depending upon their quality or noise level.

The deficiencies of diffusion tensor MRI using seven DWIs should be more pronounced in measures of diffusion anisotropy than in Trace($\underline{D}$). First, to calculate Trace($\underline{D}$), we add all six log-ratio images, so errors will tend to cancel. Measures of anisotropy, such as RA, depend on squares of diagonal and off-diagonal elements of $\underline{D}$ (5) whose errors due to noise are rectified. Thus, anisotropy indices such as the RA are intrinsically more susceptible to noise contamination than is Trace($\underline{D}$), as reflected in their larger bias and error variance at the same levels of the signal-to-noise ratio (6). Given that the signal-to-noise ratio in many clinical imagers is usually low, and peak diffusion gradients are often $<1$ G/cm, in this case, Figs. 3a and 3b are more representative of the quality of the RA anisotropy indices one would expect to obtain using the seven DWI method than is Fig. 3d. Monte Carlo simulations of DT-MRI experiments also suggest that the bias and error variance of these measures would be

unacceptably high for clinical applications using presently available clinical hardware (6). Calculating a lattice anisotropy index (6) from the set of seven DWIs ameliorates the problem of susceptibility to thermal noise but generally does not correct for systematic artifacts.

The *a priori* assumption that diffusion is cylindrically symmetric in tissues (18, 35, 36) (i.e., that two principal diffusivities are equal in a voxel), is explicitly not made here. Recent experimental findings in normal human brain (7) show that this assumption is not satisfied in the majority of white matter regions (in particular, in the fibers in the centrum semiovale). Similar findings have been published for cardiac muscle (12). Instead of invoking diffusion symmetry *a priori*, it is preferable to first measure the entire diffusion tensor and then test for symmetry *a posteriori* (37). Diffusion tensor MRI using seven DWIs does not preclude using this approach.

## SUMMARY

In performing diffusion tensor MRI with seven DWIs, one uses the fewest DWIs consistent with the assumption that water diffusion in the tissue is fully anisotropic. In this case, simple analytical expressions can be derived for $\underline{D}$ as well as for quantities derived from it. Using only seven DWIs also reduces the total scan time, as well as the complexity and time of postprocessing the DWIs. However, this method, like other simplified diffusion tensor MRI schemes, does not provide estimates of moments (e.g., mean and variance) of the diffusion tensor or of other parameters derived from it. Moreover, these simplified methods are generally more susceptible to background noise contamination and to systematic artifacts. Consequently, care must be exercised when using any of these simplified imaging schemes in radiological applications.

## ACKNOWLEDGMENTS

The authors thank Barry Bowman and Z. and R. Bigio for editing this manuscript.

## REFERENCES

1. J. Kärger, H. Pfeifer, W. Heink, Principles and applications of self-diffusion measurements by nuclear magnetic resonance, *in* "Advances in Magnetic Resonance" (Waugh J, Ed.), pp. 1–89, Academic Press, New York, 1988.
2. P. J. Basser, J. Mattiello, D. Le Bihan, MR diffusion tensor spectroscopy and imaging. *Biophys. J.* **66,** 259–267 (1994).
3. A. M. Ulug, N. Beauchamp, R. N. Bryan, P. C. M. van Zijl, Absolute quantitation of diffusion constants in human stroke. *Stroke* **28,** 483–490 (1997).
4. S. Warach, J. Gaa, B. Siewert, P. Wielopolski, R. R. Edelman, Acute human stroke studied by whole brain echo planar diffusion-weighted magnetic resonance imaging. *Ann. Neurol.* **37,** 231–241 (1995).
5. P. J. Basser, C. Pierpaoli, Microstructural and physiological features of tissues elucidated by quantitative-diffusion-tensor MRI. *J. Magn. Reson. B* **111,** 209–219 (1996).
6. C. Pierpaoli, P. J. Basser, Toward a quantitative assessment of diffusion anisotropy. *Magn. Reson. Med.* **36,** 893–906 (1996).
7. C. Pierpaoli, P. Jezzard, P. J. Basser, A. Barnett, G. Di Chiro, Diffusion tensor MR imaging of the human brain. *Radiology* **201,** 637–648 (1996).
8. C. Pierpaoli, A. Barnett, L. Penix, T. De Graba, P. J. Basser, G. Di Chiro, Identification of fiber degeneration and organized gliosis in stroke patients by diffusion tensor MRI, *in* "Proc., ISMRM, 4th Annual Meeting, New York, 1996," p. 563.
9. A. M. Ulug, O. Bahkt, R. N. Bryan, P. C. M. van Zijl, Mapping of human brain fibers using diffusion tensor imaging, *in* "Proc., ISMRM, 4th Annual Meeting, New York, 1996," p. 1325.
10. C. Pierpaoli, Oh no! One more method for color mapping of fiber tract direction using diffusion MR imaging data, *in* "Proc., ISMRM, 5th Annual Meeting, Vancouver, 1997," p. 1741.
11. D. K. Jones, S. C. R. Williams, M. A. Horsfield, Full representation of white-matter fibre direction on one map via diffusion tensor analysis, *in* "Proc., ISMRM, 5th Annual Meeting, Vancouver, 1997," p. 1743.
12. L. Garrido, V. J. Wedeen, K. K. Kwong, U. M. Spencer, H. L. Kantor, Anisotropy of water diffusion in the myocardium of the rat. *Circ. Res.* **74,** 789–793 (1994).
13. T. G. Reese, R. M. Weisskoff, R. N. Smith, B. R. Rosen, R. E. Dinsmore, V. J. Wedeen, Imaging myocardial fiber architecture in vivo with magnetic resonance. *Magn. Reson. Med.* **34,** 786–791 (1995).
14. E. C. Wong, R. W. Cox, Single-shot imaging with isotropic diffusion weighting, *in* "Proc., SMR, 2nd Annual Meeting, San Francisco, 1994," p. 136.
15. E. C. Wong, R. W. Cox, A. W. Song, Optimized isotropic diffusion weighting. *Magn. Reson. Med.* **34,** 139–143 (1995).
16. S. Mori, P. C. van Zijl, Diffusion weighting by the trace of the diffusion tensor within a single scan. *Magn. Reson. Med.* **33,** 41–52 (1995).
17. G. Liu, P. van Gelderen, J. Duyn, C. T. W. Moonen, Single-shot diffusion MRI of human brain on a conventional clinical instrument. *Magn. Reson. Med.* **35,** 671–677 (1996).
18. T. E. Conturo, R. C. McKinstry, E. Akbudak, B. H. Robinson, Encoding of anisotropic diffusion with tetrahedral gradients: a general mathematical diffusion formalism and experimental results. *Magn. Reson. Med.* **35,** 399–412 (1996).
19. R. Shrager, P. J. Basser, Anisotropically weighted MRI. *Magn. Reson. Med.*, in press.
20. P. J. Basser, R. Shrager, Anisotropically-weighted MRI, *in* "Proc., ISMRM, 5th Annual Meeting, Vancouver, 1997," p. 226.
21. P. J. Basser, J. Mattiello, D. Le Bihan, Estimation of the effective self-diffusion tensor from the NMR spin echo. *J. Magn. Reson. B* **103,** 247–254 (1994).
22. J. Mattiello, P. J. Basser, D. LeBihan, The b matrix in diffusion tensor echo-planar imaging. *Magn. Reson. Med.* **37,** 292–300 (1997).
23. J. Mattiello, P. J. Basser, D. LeBihan, Analytical expression for the b matrix in NMR diffusion imaging and spectroscopy. *J. Magn. Reson. A* **108,** 131–141 (1994).
24. J. Mattiello, P. J. Basser, D. LeBihan, Analytical calculation of the b matrix in diffusion imaging, *in* "Diffusion and Perfusion Magnetic Resonance Imaging" (LeBihan D, Ed.), pp. 77–90, Raven Press, New York, 1995.
25. T. L. Davis, V. J. Wedeen, R. M. Weisskoff, B. R. Rosen, White matter tract visualization by echo-planar MRI, *in* "Proc., SMRM, 12th Annual Meeting, New York, 1993," p. 289.
26. D. Le Bihan, Molecular diffusion nuclear magnetic resonance imaging. *Magn. Reson. Q.* **7,** 1–30 (1991).
27. W. H. Press, S. A. Teukolsky, W. T. Vetterling, B. P. Flannery, "Numerical Recipes in C," Cambridge University Press, Cambridge, 1992.
28. G. Strang, "Introduction to Applied Mathematics," Wellesley-Cambridge Press, Wellesley, 1986.
29. P. Jezzard, C. Pierpaoli, Dual-echo navigator approach to minimization of eddy current and motion artifacts in echo-planar diffusion imaging, *in* "Proc., ISMRM, 4th Annual Meeting, New York, 1996," p. 189.
30. P. Jezzard, C. Pierpaoli, Diffusion mapping using interleaved Spin Echo and STEAM EPI with navigator echo correction, *in* "Proc., SMR, 3rd Annual Meeting, Nice, France, 1995," p. 903.
31. G. Liu, P. van Gelderen, C. T. W. Moonen, Single-shot diffusion MRI on a conventional clinical instrument, *in* "Proc., SMR, 2nd Annual Meeting, San Francisco, 1994," p. 1034.
32. C. Pierpaoli, C. Baratti, P. Jezzard, Fast tensor imaging of water diffusion changes in gray and white matter following cardiac arrest in cats, *in* "Proc., ISMRM, 4th Annual Meeting, New York, 1996," p. 314.
33. M. Neeman, J. P. Freyer, L. O. Sillerud, Pulsed-gradient spin-echo studies in NMR imaging; effects of the imaging gradients on the determination of diffusion coefficients. *J. Magn. Reson.* **90,** 303–312 (1990).
34. D. Chien, R. B. Buxton, K. K. Kwong, T. J. Brady, B. R. Rosen, MR diffusion imaging of the human brain. *J. Comput. Assist. Tomogr.* **14,** 514–520 (1990).
35. E. W. Hsu, S. Mori, Analytical expressions for the NMR apparent diffusion-coefficients in an anisotropic system and a simplified method for determining fiber orientation. *Magn. Reson. Med.* **32,** 194–200 (1995).
36. J. Coremans, R. Luypaert, F. Verhelle, T. Stadnik, M. Osteaux, A method for myelin fiber orientation mapping using diffusion-weighted MR images. *Magn. Reson. Imaging* **12,** 443–454 (1994).
37. P. J. Basser, Testing for and exploiting microstructural symmetry to characterize tissues via diffusion tensor MRI. *in* "Proc., ISMRM, 4th Annual Meeting, New York, 1996," p. 1323.